Journal of Power Sources 218 (2012) 113–118

Contents lists available at SciVerse ScienceDirect

Journal of Power Sources

journal homepage: www.elsevier.com/locate/jpowsour

Electrochemical decomposition of Li_2CO_3 in NiO–Li_2CO_3 nanocomposite thin film and powder electrodes

Rui Wang [a], Xiqian Yu [a,b], Jianming Bai [c], Hong Li [a,*], Xuejie Huang [a], Liquan Chen [a], Xiaoqing Yang [b]

[a] Institute of Physics, Chinese Academy of Sciences, Beijing 100190, PR China
[b] Brookhaven National Laboratory, Upton, NY 11973, USA
[c] Oak Ridge National Laboratory, Oak Ridge, TN 37831, USA

HIGHLIGHTS

- NiO–Li_2CO_3 composite thin film and powder electrodes are prepared.
- Li_2CO_3 phase is decomposable after being charging to 4.1 V.
- NiO acts as a catalyst to decompose Li_2CO_3.

ARTICLE INFO

Article history:
Received 13 June 2011
Received in revised form
6 December 2011
Accepted 22 June 2012
Available online 2 July 2012

Keywords:
Lithium carbonate
Nickel oxide
Nanocomposite
Decomposition
Thin film
Lithium ion batteries

ABSTRACT

Two types of NiO–Li_2CO_3 nanocomposite electrodes have been prepared for the electrochemical decomposition studies. The thin film electrode with a thickness of 225 nm and grain size around 5–8 nm is prepared by a pulsed laser deposition method. The powder sample is prepared by a solution evaporation and calcination method with primary particle size in the range of 20–50 nm. Using *ex situ* TEM, Raman and FTIR spectroscopy and synchrotron based *in situ* XRD, the electrochemical decomposition of Li_2CO_3 phase in both types of the NiO–Li_2CO_3 nanocomposite electrodes after charging up to about 4.1 V vs Li^+/Li at room temperature is clearly confirmed, but not in the electrode containing only Li_2CO_3. The NiO phase does not change significantly after charging process and may act as catalyst for the Li_2CO_3 decomposition. The potential of using NiO–Li_2CO_3 nanocomposite material as additional lithium source in cathode additive in lithium ion batteries has been demonstrated, which could compensate the initial irreversible capacity loss at the anode side.

1. Introduction

Since the first report on reversible heterogeneous lithium storage in transition metal oxides by Poizot et al. in 2000 [1], the mechanism of conversion reaction has attracted a lot of attention. It is fundamentally interesting that the inert Li_2O is electrochemically decomposable at room temperature when forming nanocomposite with transition metals (TM). Later, analogous reversible lithium storage was also observed in transition metal fluorides, sulfides, nitrides, phosphides and selenides [2–7]. The enhanced electrochemical reactivity of LiX (X = F, O, S, N, P) is mainly related to the nanocomposite microstructure where the LiX and TM phases have extremely small grain size (<5 nm) and disperse uniformly. It is also noticed that the solid electrolyte interphase (SEI) on these materials is decomposable upon charging [1,8–10]. This is quite different than the case of the SEI film on the graphite anode [11,12]. Our previous investigations confirmed that the oligomer, lithium alkyl carbonate and polymer like SEI components on Cr_2O_3 anode are not stable after charging to 3.0 V [9]. It is well known that inorganic phases, such as Li_2O, LiF and Li_2CO_3 are important components in the SEI films. Since Li_2O or LiF can be electrochemically decomposed in the conversion reaction on transitional metal compound anodes, it is very important to see if Li_2CO_3 is also electrochemically decomposable in its nanocomposite with transitional metal or metal compounds. Recently, reversible lithium storage in $MnCO_3$ in a voltage range of 0–3.0 V vs Li^+/Li was reported by Tirado et al [13,14]. A conversion reaction mechanism was proposed but no experimental evidences were provided. This implies the possible decomposition of Li_2CO_3 when forming nanocomposite with Mn.

* Corresponding author. Tel.: +86 10 82648067; fax: +86 10 82649046.
E-mail address: hli@iphy.ac.cn (H. Li).

0378-7753/$ – see front matter © 2012 Elsevier B.V. All rights reserved.
http://dx.doi.org/10.1016/j.jpowsour.2012.06.082

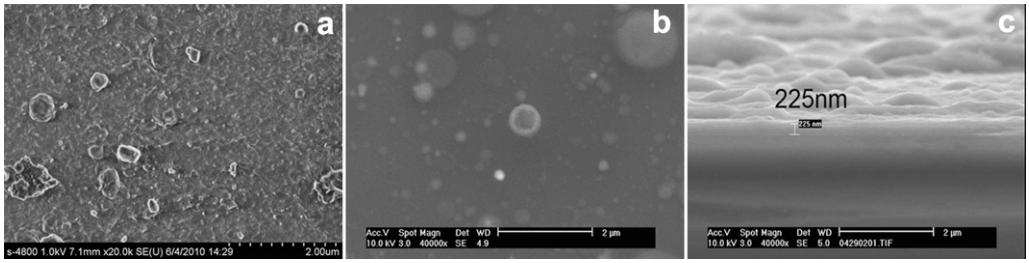

Fig. 1. (a and b) Top view of SEM images of the NiO–Li_2CO_3 composite thin films on Ti and Si substrates, respectively. (c) Cross-section view of the film on Si substrate.

It is also known that Li_2CO_3 phase can be found on the surface of Ni-based $LiMO_2$ type layered cathode materials after exposing in air for long time [15–17]. The existence of Li_2CO_3 on the surface of cathode materials produces severe deleterious effects on the capacity and power performance of the cathodes [16,17]. It has been noticed that aged Ni-based $LiMO_2$ shows an irreversible capacity loss. The origin is suggested to be related to the electrolyte decomposition. However, it is not clear whether the capacity loss is also related to the irreversible decomposition of Li_2CO_3.

In addition, it was regarded that the poor cycle life of the Li-air batteries using carbonate-based electrolytes is probably due to the undesirable discharge products of carbonates (lithium alkyl carbonates and/or Li_2CO_3) rather than the desired Li_2O_2 and Li_2O [18–20]. Therefore, the electrochemical decomposition of Li_2CO_3 could be applied in a positive way for the Li-air batteries.

Accordingly, the studies on electrochemical decomposition of Li_2CO_3 will have very important implication for both Li-ion batteries and Li-air batteries. In this work, the NiO–Li_2CO_3 thin films and powder nanocomposite electrode have been prepared and characterized by SEM, XRD, TEM, Raman, and FTIR. The electrochemical decomposition phenomenon of Li_2CO_3 in the nanocomposite electrodes is investigated.

2. Experimental

The NiO–Li_2CO_3 nanocomposite thin film electrodes were prepared by a pulsed laser deposition (PLD) system. A mixture of NiO (99%, Sinopharm Chemical Reagent Co., Ltd) and Li_2CO_3 (98%, Sinopharm Chemical Reagent Co., Ltd) at a molar ratio of 1:1.1 was ball-milled for 6 h, and then pressed into a one-inch diameter pellet. The pellet was then sintered at 450 °C under argon atmosphere for 24 h to form a PLD target. In the PLD system, a KrF excimer laser (Tuilaser, 248 nm beam, Germany) was used as a light source. The laser beam was focused on the rotating NiO–Li_2CO_3 target with an angle of 45°, and the target–substrate distance was 35 mm. The energy density was fixed at 5 J cm^{-2} with a repetition rate of 9 Hz. Before deposition, the PLD chamber was evacuated to 1.0×10^{-4} Pa and then kept at 20 Pa under high-purity argon (99.999%) during deposition. The thin film was deposited for 1.5 h on two different types of substrates: on Ti foil (99.99%, Alfa, polished by 1000 # sand paper) at RT for Raman, Fourier transformed infrared (FTIR), scanning electron microscopy (SEM), transmission electron microscopy (TEM), and electrochemical studies; and on Si (100) wafer for thickness measurements.

The NiO–Li_2CO_3 composite powder was synthesized as follows. Firstly, 6.242 g of $C_4H_6NiO_4 \cdot 4H_2O$ (99%, Sinopharm Chemical Reagent Co., Ltd) and 5.075 g of $C_2H_3LiO_2 \cdot 2H_2O$ (98%, Shanghai Huajing Biological High-Tech Co., Ltd) were dissolved in 100 ml of distilled water, then 100 ml aqueous solution contained 0.075 M NH_4HCO_3 (AR, Beijing Chemical Reagents Company) was dripped in the pre-blended solution. The suspension was kept stirring for 1 h after the addition, and then was dried at 80 °C for about 72 h. The as-prepared powders were ground and heated in air at 400 °C for 1 h. The final product, the NiO–Li_2CO_3 composite material, was ground and used for further tests. The NiO–Li_2CO_3 powder electrodes were composed of the NiO–Li_2CO_3 powder, carbon black and PVDF at a weight ratio of 80:10:10. An Al foil was used as current collector and the electrode area was 0.64 cm^2 (8 × 8 mm). The electrochemical experiments for both the powder and the thin film electrodes were performed using Swagelok type two-electrode cells. The electrolyte was 1 M $LiPF_6$ dissolved in ethylene carbonate (EC) and dimethyl carbonate (DMC) with a volume ratio of 1:1 (Shanghai Topsol Ltd., H_2O < 5 ppm). The cells were assembled in an argon-filled glove box and cycled using a Land automatic battery tester. The thin films and powders were analyzed by an X'Pert Pro MPD X-ray diffracter (Philips, Holland) using Cu Kα1 radiation (λ = 1.5405 Å), a micro-Raman spectrometer (Horiba/Jobin Yvon HR800, France) with a 532 nm laser line, a scanning electron (SEM) microscope (XL 30 S-FEG, FEI Co., USA or Hitachi S4800, Hitachi, Japan), and a transmission electron (TEM) microscope (FEI Tecnai F-20). The sample for TEM investigation was prepared by scratching the surface of the thin film using stainless steel doctor blade and dispersing the scrapings into dimethyl carbonate then transferring onto holey carbon Cu grids in the glove box. Each Fourier transformed infrared (FTIR) spectrum was taken as the average of 400 scans on a BIO-RAD FTS-60 spectrometer. The investigation of *in situ* XRD pattern was accomplished on the beam line X14A with the energy of 16 keV (0.776 Å) at the National Synchrotron Light Source (NSLS), Brookhaven National Laboratory, USA. The optics was designed to focus the beam into

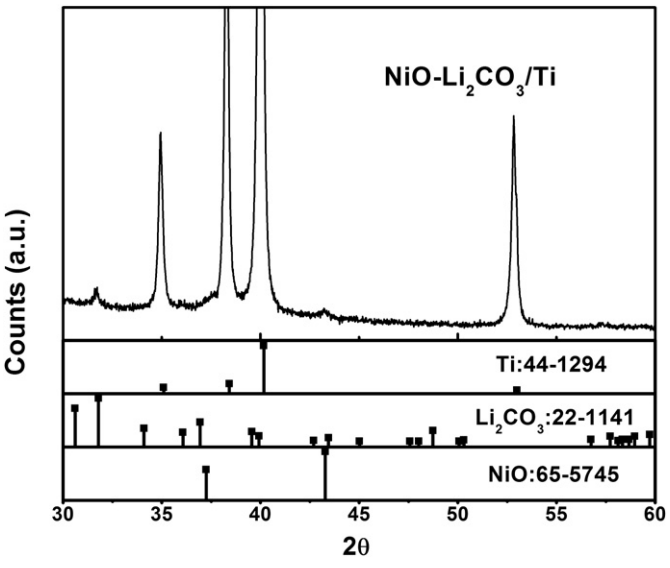

Fig. 2. XRD pattern of NiO–Li_2CO_3 nanocomposite thin film.

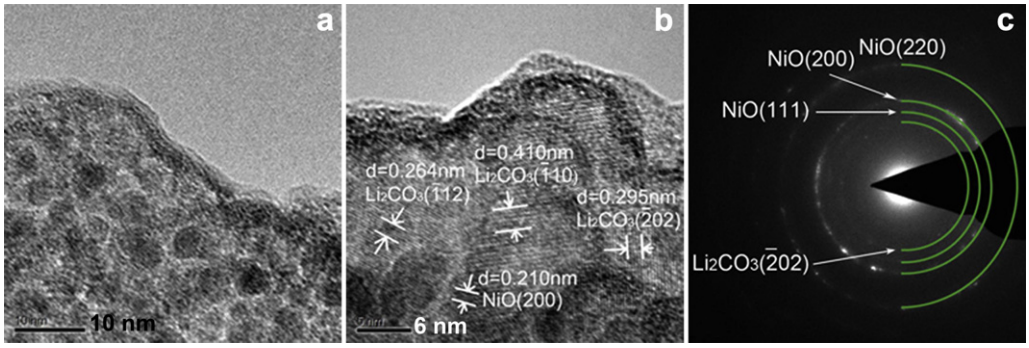

Fig. 3. TEM images (a and b) and SAED pattern (c) of the NiO–Li_2CO_3 (1:1.1) composite thin film deposited at room temperature.

a 1.75 mm × 1 mm spot size at the middle of the 2032 coin cell, and data was collected by using a linear position sensitive silicon detector. The cell was charged to 4.7 V with current density of 22 mA g^{-1}.

3. Results and discussion

3.1. Characterization of as-deposited NiO–Li_2CO_3 composite thin films

Fig. 1a and b show the typical scanning electron micrographs of the deposited NiO–Li_2CO_3 films on Ti and Si substrates, respectively. It can be seen that there are many particles up to several micrometers spread around on the surface. EDX mapping results (not shown) indicate that Ni, C, O and Ti coexist in this film and these elements distributed in the film uniformly, even on the big particles. The cross-section image of the film deposited on Si in Fig. 1c reveals that the thin film is continuous and dense, though the surface is not smooth. The thickness of the dense part is about 225 nm.

XRD pattern of the NiO–Li_2CO_3 composite thin film on the Ti substrate is shown in Fig. 2. The diffraction peaks of the Ti substrate can be seen clearly. Besides, only the strongest peaks of Li_2CO_3 at 2θ of 31.84° and NiO at 2θ of 43.39° can be identified, respectively. The broad peaks indicate that the NiO and Li_2CO_3 in the films should be at a form of nanocrystalline.

The formation of the NiO–Li_2CO_3 nanocomposite in the film is confirmed by the high-resolution TEM image. A typical TEM image from the as-deposited NiO–Li_2CO_3 nanocomposite thin film is shown in Fig. 3a, in which many tiny crystalline grains with a grain size of 5–8 nm can be observed. Clear lattice stripes can be also seen in the HRTEM image (Fig. 3b). The SAED pattern shown in Fig. 3c exhibits clear rings made up of discrete spots. All *d*-spacings derived from the SAED pattern can be assigned to NiO and Li_2CO_3. Thus, the prepared film is a NiO–Li_2CO_3 nanocomposite thin film.

3.2. Electrochemical characteristics at the voltage range of 4.3–2 V

The thin films of NiO, Li_2CO_3, and NiO–Li_2CO_3 were deposited under the same deposition condition on Ti substrates at room temperature for electrochemical measurements. Their charge and discharge curves in lithium cells in the range of 4.3–2 V are shown in Fig. 4. The NiO thin film electrode shows sloped voltage profiles with an initial charge capacity of about 9 mAh (g NiO)$^{-1}$ estimated using the thickness of 163 nm and the density of 6.8 gcm^{-3}. The measured capacity may originate from the surface charging effect. The Li_2CO_3 island-like thin film electrode with a thickness about 400 nm shows even poorer reactivity. As for the NiO–Li_2CO_3 composite thin film, the voltage profile shows a clear charge plateau at about 4.1 V vs Li^+/Li at the first cycle and it is irreversible. According to a rough estimation assuming the molar ratio of NiO to Li_2CO_3 in the thin film is the same as the molar ratio of the target (the real composition is hard to be determined accurately by EDX for the thin film electrode) and the density of the film is an average density of 3.1 gcm^{-3} for the mixture of the NiO and Li_2CO_3 (1:1.1 in molar ratio), the initial charge capacity is about 362 mAh (g NiO–Li_2CO_3)$^{-1}$, which is quite close to the theoretical capacity of 379 mAh g^{-1} if all the Li_2CO_3 phase in the nanocomposite thin film is decomposed. Therefore, the irreversible charge voltage plateau is proposed to be related to the electrochemical decomposition of the Li_2CO_3 phase. In order to verify this, Raman, FTIR, and TEM investigations are performed on the NiO–Li_2CO_3 nanocomposite thin film electrodes before and after the initial charge.

Raman spectra of the thin film electrodes are shown in Fig. 5. Characteristic band at 517 cm^{-1} for the longitudinal optical phonon mode of NiO and 1090 cm^{-1} for the carbonyl symmetric stretching

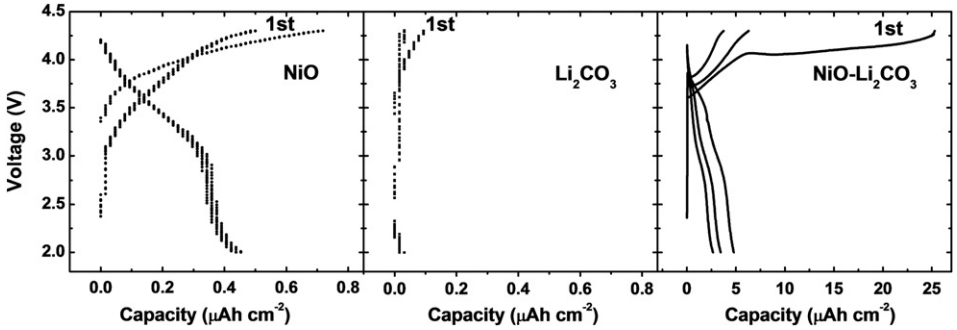

Fig. 4. Charging and discharging curves of the NiO, Li_2CO_3, and NiO–Li_2CO_3 composite thin films on Ti pellet electrodes at room temperature. The electrode area was 0.64 cm^2. Current: 1 μA.

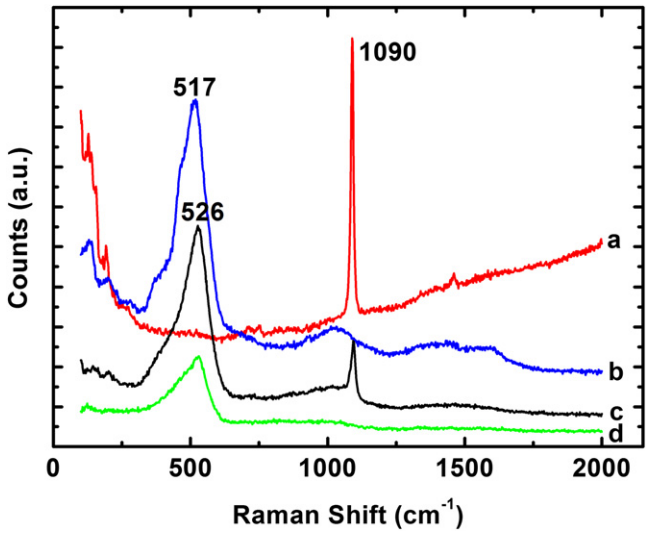

Fig. 5. Raman spectra of the a) Li_2CO_3, b) NiO, c) NiO–Li_2CO_3 composite electrode and d) the NiO–Li_2CO_3 composite films after the initial charging.

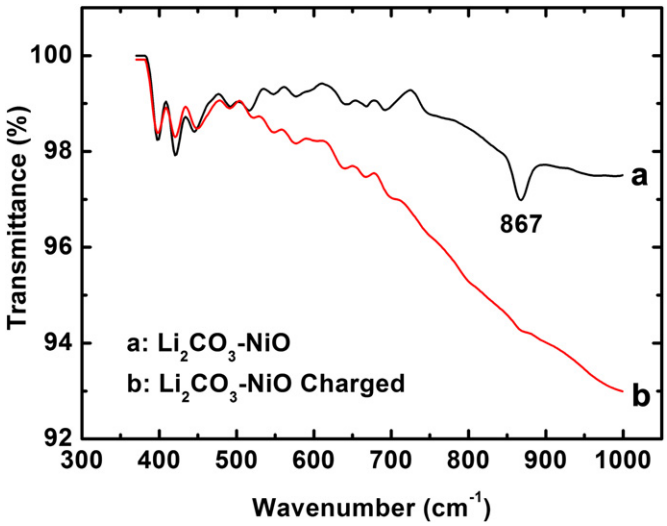

Fig. 6. FTIR spectra of the NiO–Li_2CO_3 composite electrode films a) before and b) after the initial charge.

vibration mode of Li_2CO_3 can be seen clearly in the Raman spectra of the NiO and Li_2CO_3 films respectively, consistent with earlier reports [21,22]. As for the NiO–Li_2CO_3 composite film, both bands can be seen in the Curve C. This confirms further that the as-deposited film is composed of the two phase of NiO and Li_2CO_3. After charging to 4.3 V vs Li^+/Li, it can be seen that only the band from NiO is remained and the characteristic band of Li_2CO_3 disappears. This confirms that the Li_2CO_3 phase in the nanocomposite thin film electrode is decomposed after the first charge.

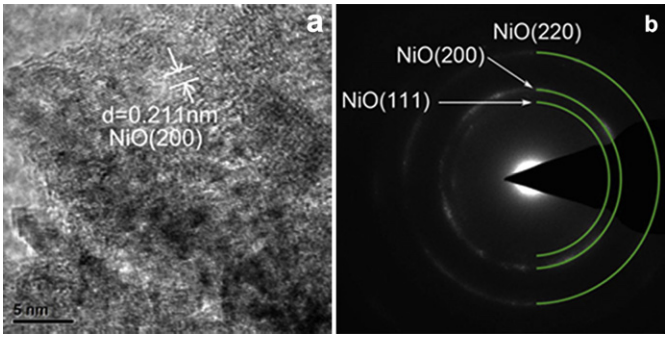

Fig. 7. (a) *Ex situ* TEM image of the as-deposited NiO–Li_2CO_3 nanocomposite thin film after being charged to 4.3 V; (b) the corresponding SAED pattern.

Fig. 6 compares the FTIR spectra of the pristine NiO–Li_2CO_3 composite thin film electrode and the one after being charged to 4.3 V vs Li^+/Li. Comparing the FTIR spectra of the electrodes before and after initial charge, it can be seen that the characteristic absorbance band of Li_2CO_3 at 867 cm^{-1} [17] disappears after the cell is charged to 4.3 V. This is consistent with the Raman spectroscopy investigation.

When the thin film electrode is charged to 4.3 V, many stripes are observed in the TEM image as shown in Fig. 7a. The distance between all parallel stripes is about 0.211 nm, consistent with the *d*-spacing of 0.209 nm for (200) of cubic NiO (JCPDS 75-0197). The *d*-spacings in the SAED patterns in Fig. 7b are 0.249, 0.214, 0.151 nm, consistent with *d*-values of (111), (200) and (220) plane of cubic NiO. In all the observed regions, SAED patterns of the Li_2CO_3 phase cannot be found. It indicates further that Li_2CO_3 is decomposed after initial charge.

3.3. Characterization and electrochemical performance of the NiO–Li_2CO_3 composite powder electrode

The primary and secondary particle size range of obtained NiO–Li_2CO_3 composite powder sample is about 20–50 nm and 200–500 nm, as shown in Fig. 8a and b respectively. XRD pattern of the NiO–Li_2CO_3 composite powder is shown in Fig. 9. The diffraction peaks of NiO and Li_2CO_3 can be seen clearly. Grain size is roughly 40 nm, roughly estimated from Scherrer equation. In addition, it is noticed that metallic nickel also exists, which could be due to the reduction effect of organic precursors on NiO although

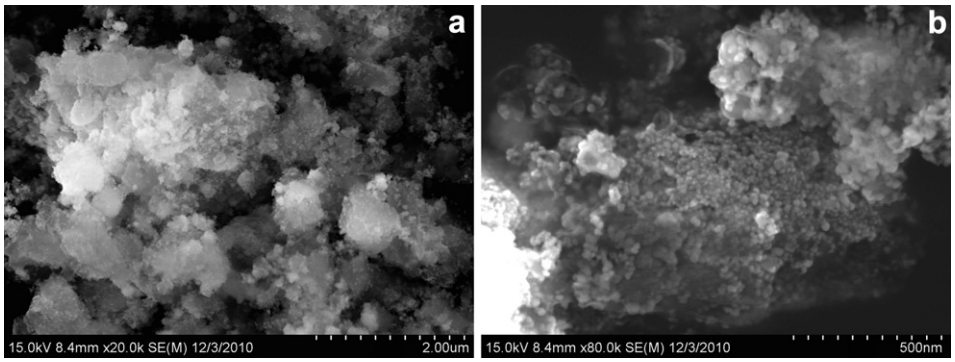

Fig. 8. SEM images of the NiO–Li_2CO_3 composite powder at different magnifications.

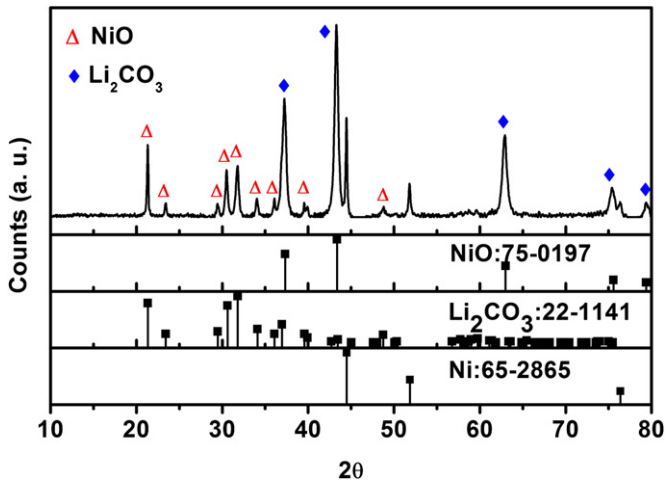

Fig. 9. XRD patterns of NiO–Li_2CO_3 composite powder.

the sample was sintered in air at 400 °C for 1 h. For convenience, the sample is still named as the NiO/Li_2CO_3 composite.

Fig. 10 shows the voltage profiles of the NiO–Li_2CO_3 composite powder electrode between 4.5 V and 2 V. It can be seen that the material has a charge capacity of 240 mAh (g NiO–Li_2CO_3)$^{-1}$ at 4.4 V and a discharge capacity of 7 mAh g^{-1} at the first cycle. From the second cycle, the charge capacity drops to 20 mAh g^{-1}. This phenomenon is similar to the NiO–Li_2CO_3 nanocomposite film. However, perhaps due to large particle size and grain size, the kinetic property of the powder electrode is worse than the thin film electrode. The charge voltage is increased to 4.4 V and the charge capacity is decreased.

As shown in the *in situ* XRD patterns in Fig. 11, during charging, the relative intensity of the diffraction peaks of Al foils, Ni and NiO for the composite powder electrode does not change. However, the intensities of characteristic peaks for Li_2CO_3 are decreased gradually. This further confirms clearly that the Li_2CO_3 phase is electrochemically decomposed and the NiO/Ni phase in the nanocomposite acts as catalysts for the decomposition reaction. It should be mentioned that the Li_2CO_3 powder electrode without NiO/Ni only showed a charge capacity of 6.9 mAh g^{-1}. It indicates further that NiO/Ni plays an important role as catalyst in this electrochemical decomposition.

Above results indicate unambiguously that Li_2CO_3 in the NiO–Li_2CO_3 nanocomposite is decomposed after charging to 4.1 V vs Li^+/Li and the NiO phase or NiO/Ni phase in the nanocomposite may play an important role as catalyst. The decomposition of Li_2CO_3 may take place through two reactions:

$$Li_2CO_3 \rightarrow 2e^- + 2Li^+ + 1/2O_2 + CO_2 \quad (1)$$

$$Li_2CO_3 \rightarrow Li_2O + CO_2 \quad (2)$$

$$\Delta_f G(Li_2CO_3) = -1132.12 \text{ kJ mol}^{-1}$$

$$\Delta_f G(CO_2) = -457.2 \text{ kJ mol}^{-1} \quad [23]$$

EMF = 3.50 V vs Li^+/Li

The standard Gibbs formation energy of Li_2CO_3 ($\Delta_f G^0(Li_2CO_3)$) is −1132.12 kJ mol^{-1} [23], the standard free enthalpy of CO_2 ($\Delta_f H^0(CO_2)$) is −393.5 kJ mol^{-1} [23], the standard entropy of CO_2 ($\Delta_f S^0$ (CO_2)) = 213.8 J mol^{-1} K^{-1} [23]. The standard formation energy for reaction (1) is 674.9 kJ mol^{-1}. According to Nernst equation, the emf value of this reaction is 3.50 V. The standard formation energy for reaction (2) is 113.8 kJ mol^{-1}. Reaction (2) is not an electrochemical reaction and is not able to take place spontaneously at room temperature. Therefore, the reaction mechanism (1) is much plausible. Further studies on the role of NiO as a catalyst and the release of O_2 and CO_2 for this Li_2CO_3 electrochemical decomposition will be performed in near future.

Since Li_2CO_3 can be decomposed irreversibly, we propose that the NiO–Li_2CO_3 composite material could be considered as an additive to compensate the initial irreversible capacity loss for some high capacity anode materials in Li-ion batteries. Since the lithium consumed through this irreversible reaction will no longer be available for subsequent cycling, additional lithium source is needed to compensate it. For a preliminary demonstration, the NiO–Li_2CO_3 composite powder is mixed with commercial $LiMn_2O_4$ powder at a weight ratio of 1:1 as cathode. As shown in Fig. 12, after the addition of NiO–Li_2CO_3 nanocomposite, the charge capacity in the initial cycle has risen from ~120 mAh g^{-1} to ~410 mAh g^{-1} (calculated according to the mass of $LiMn_2O_4$ in the cathode). At the

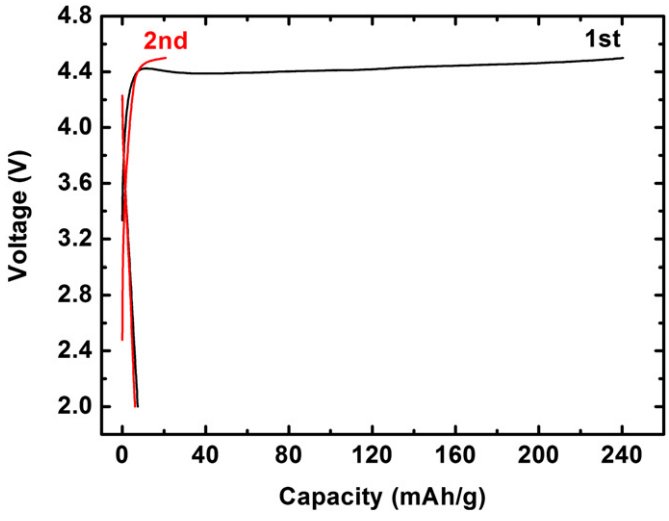

Fig. 10. Charging and discharging curves of the NiO–Li_2CO_3 composite powder electrode. The electrode area was 0.64 cm^2. Current: 10 mA g^{-1}.

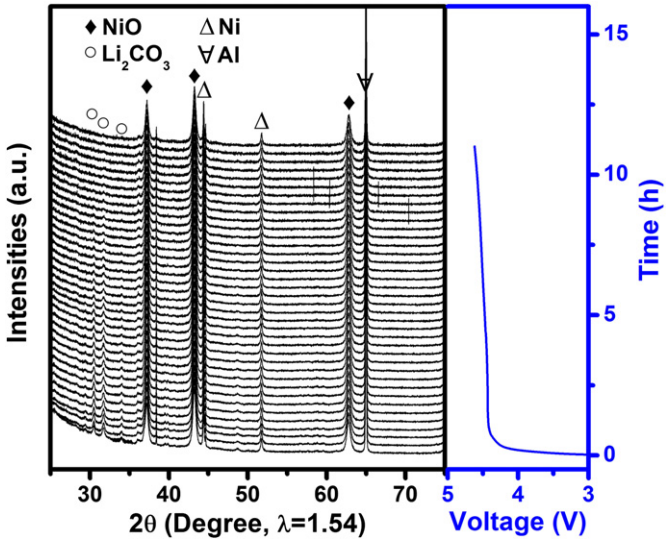

Fig. 11. *In situ* XRD patterns of the NiO–Li_2CO_3 composite powder electrode.

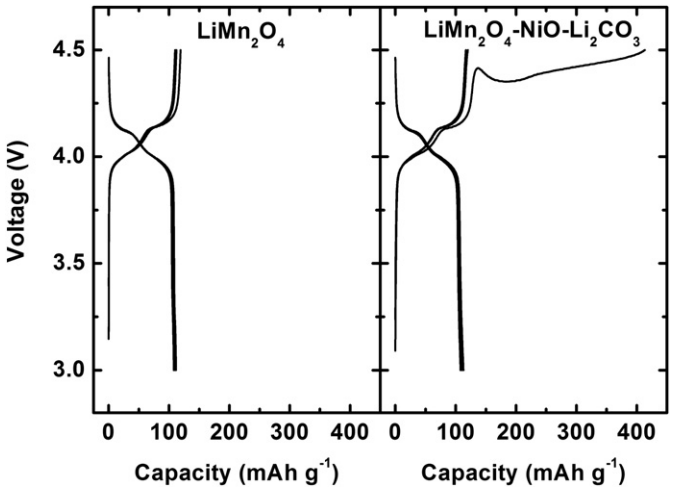

Fig. 12. Charging and discharging curves of the $LiMn_2O_4$ and $LiMn_2O_4$–NiO–Li_2CO_3 electrodes, the electrode area was 0.64 cm^2. Current: 5 mA g^{-1}. Capacity is calculated based on the weight of $LiMn_2O_4$ in both cases.

same time, the discharge capacity doesn't have any change, which means the decomposition reaction of Li_2CO_3 has supplied an irreversible capacity of nearly ~300 mAh g^{-1} in the first cycle. And this substantial amount of additional lithium source can compensate the Li-consumption at anode. The cyclic performance and capacity of $LiMn_2O_4$ is not influenced. For practical application, the adding of the NiO/Li_2CO_3 nanocomposite will release extra CO_2 and O_2 at the first cycle. This issue can be solved by "degassing" procedure during battery formation, which has been widely used in industry.

4. Conclusions

It is confirmed that the Li_2CO_3 phase in the NiO–Li_2CO_3 nanocomposite in both thin film and powder electrodes can be electrochemically decomposed above 4.1 V vs Li^+/Li and the NiO phase may act as the catalyst. This electrochemical decomposition has been confirmed by *ex situ* TEM, Raman and FTIR and synchrotron based *in situ* XRD studies. The irreversible electrochemical decomposition of Li_2CO_3 in the nanocomposite may have the potential to be used as a new lithium compensation additive in cathode for Li-ion batteries. This finding could be also relevant for design the air electrode in order to decompose the side product of Li_2CO_3 in nonaqueous Li-air batteries.

Acknowledgments

Financial supports from CAS (KJCX2-YW-W26), NSFC (50730005), "863" project (2009AA033101) and "973" project (2007CB936501) are appreciated. Work at BNL is supported by the Assistant Secretary for Energy Efficiency and Renewable Energy, Office of Vehicle Technologies, under the program of Vehicle Technology Program, under Contract Number DEAC02-98CH10886. Research at beam line X14A was partially sponsored by the U.S. DOE, Office of EERE, Vehicle Technologies Program, through the ORNL's High Temperature Materials Laboratory User Program. The authors thank the help from Dr. Yanyan Liu for SEM investigation.

References

[1] P. Poizot, S. Laruelle, S. Grugeon, L. Dupont, J.M. Tarascon, Nature 407 (2000) 496–499.
[2] H. Li, G. Richter, J. Maier, Adv. Mater. 15 (2003) 736–739.
[3] F. Badway, N. Pereira, F. Cosandey, G.G. Amatucci, J. Electrochem. Soc. 150 (2003) A1209–A1218.
[4] D.C.C. Silva, O. Crosnier, G. Ouvrard, J. Greedan, A. Safa-Sefat, L.F. Nazar, Electrochem. Solid State Lett. 6 (2003) A162–A165.
[5] Y. Wang, Z.W. Fu, X.L. Yue, Q.Z. Qin, J. Electrochem. Soc. 151 (2004) E162–E167.
[6] P. Balaya, H. Li, L. Kienle, J. Maier, Adv. Funct. Mater. 13 (2003) 621–625.
[7] M.Z. Xue, Y.N. Zhou, B. Zhang, L. Yu, H. Zhang, Z.W. Fu, J. Electrochem. Soc. 153 (2006) A2262–A2268.
[8] J. Hu, H. Li, X.J. Huang, L.Q. Chen, Solid State Ionics 177 (2006) 2791–2799.
[9] Y. Zeng, L.F. Li, H. Li, X.J. Huang, L.Q. Chen, Ionics 15 (2009) 91–96.
[10] K.F. Zhong, X. Xia, B. Zhang, H. Li, Z.X. Wang, L.Q. Chen, J. Power Sources 195 (2010) 3300–3308.
[11] R. Fong, U. Vonsacken, J.R. Dahn, J. Electrochem. Soc. 137 (1990) 2009–2013.
[12] D. Aurbach, Y. Eineli, O. Chusid, Y. Carmeli, M. Babai, H. Yamin, J. Electrochem. Soc. 141 (1994) 603–611.
[13] M.J. Aragón, C.P. Vicente, J.L. Tirado, Electrochem. Commun. 9 (2007) 1744–1748.
[14] M.J. Aragón, B. León, C.P. Vicente, J.L. Tirado, J. Power Sources 196 (2011) 2863–2866.
[15] K. Matsumoto, R. Kuzuo, K. Takeya, A. Yamanaka, J. Power Sources 81 (1999) 558–561.
[16] H.S. Liu, Z.R. Zhang, Z.L. Gong, Y. Yang, Electrochem. Solid State Lett. 7 (2004) A190–A193.
[17] G.V. Zhuang, G.Y. Chen, J. Shim, X.Y. Song, P.N. Ross, T.J. Richardson, J. Power Sources 134 (2004) 293–297.
[18] F. Mizuno, S. Nakanishi, Y. Kotani, S. Yokoishi, H. Iba, Electrochemistry 78 (2010) 403–405.
[19] J. Xiao, J. Hu, D. Wang, D. Hu, W. Xu, G.L. Graff, Z. Nie, J. Liu, J.G. Zhang, J. Power Sources 196 (2011) 5674–5678.
[20] W. Xu, V.V. Viswanathan, D. Wang, S.A. Towne, J. Xiao, Z. Nie, D. Hu, J.G. Zhang, J. Power Sources 196 (2011) 3894–3899.
[21] W.Z. Wang, Y.K. Liu, C.K. Xu, C.L. Zheng, G.H. Wang, Chem. Phys. Lett. 362 (2002) 119–122.
[22] P. Pasierb, S. Komornicki, M. Rokita, M. Rekas, J. Mol. Struct. 596 (2001) 151–156.
[23] M. Binnewies, E. Milke, Thermochemical Data of Elements and Compounds, second, revised and extended ed. Wiley-VCH, Weinheim, 2002.